07,08

Phase-field simulation of two-dimensional material formation during epitaxial growth

© P.E. L'vov[1,2], A.I. Kochaev[1,3]

[1] Ulyanovsk State University,
Ulyanovsk, Russia
[2] Institute of Nanotechnology of Microelectronics, Russian Academy of Sciences,
Moscow, Russia
[3] National Research Nuclear University „MEPhI",
Moscow, Russia

E-mail: LvovPE@ulsu.ru

Received September 18, 2025
Revised October 9, 2025
Accepted October 11, 2025

In this study, we develop a phase-field model of the formation of two-dimensional (2D) materials during epitaxial growth. The model accounts for the anisotropy of boundary energy, thermal fluctuations, and the presence of continuous deposition and evaporation of atoms from the substrate surface. We investigate the formation of islands with hexagonal and triangular geometry proper to 2D materials, as well as the processes of their growth and coalescence up to the formation of a solid film. During the coalescence of two or more islands, we observed the formation of structure defects, which exhibit non-equilibrium character and gradually relax to an equilibrium shape. Some regularities of the dynamics of average size, surface number density, and size distribution function of islands are investigated.

Keywords:: phase-field theory, 2D-materials, epitaxial growth, anisotropy of the boundary energy, faceting.

DOI: 10.61011/PSS.2025.10.62639.257-25

1. Introduction

Epitaxial growth is a critical mechanism in film formation used for targeted synthesis of various two-dimensional materials. With its help, it became possible to obtain high-quality samples of various two-dimensional materials, which include graphene [1,2] and graphene-like materials [3,4], a group of borophene nano-allotropes [5,6], pseudo-two-dimensional di-chalcogenides of transition metals (MoS_2, WTe_2 and etc.) [7,8], monolayer of hexagonal boron nitride (h-BN) [9] and etc. The unique properties of two-dimensional materials — their atomic fineness, flexibility, and lack of bulk structure — lead to unusual electronic, optical, and mechanical characteristics unattainable in their three-dimensional counterparts. This gives prospects for the creation of ultralight and flexible electronics, highly efficient sensors and new generations of energy storage devices. For example, graphene with its record-hitting mobility of charge carriers is considered as the basis for fabrication of post-silicon transistors [10], semiconductor dichalcogenides may be used in ultrathin and flexible displays and photodetectors [11], while borophene, due to its high electrical conductivity, mechanical flexibility and low density, is found promising in the development of new generation batteries, catalytic reactions and hydrogen storage [12]. On the basis of two-dimensional materials, a wide variety of vertical and horizontal heterostructures can be synthesized [13–16], as well as composite materials for various purposes [1,17,18].

The mechanism of epitaxial growth is most often used in the controlled synthesis of high-quality two-dimensional materials used for basic research and prototyping of electronic devices [1,2,7,19]. The current state-of-the-art synthesis processes allow for the epitaxial growth of two-dimensional materials using chemical vapor deposition (CVD). This process involves the deposition of atoms from the gas phase onto the substrate during chemical reactions, which leads to the formation and growth of oriented islands (sheets) of two-dimensional material. The search for optimal synthesis modes for two-dimensional materials with the necessary properties requires in-depth theoretical analysis on various spatial and temporal scales, which is achieved by various methods. The structural, electronic, optical, as well as some mechanical and piezoelectric properties of known and predicted two-dimensional materials are reliably predicted using *ab initio* calculation methods [20,21]. The process of forming two-dimensional materials can be studied using the molecular dynamics method or the Monte Carlo method, which actually consider the processes of motion and interaction of individual atoms, which imposes significant requirements on the quality of interatomic interaction potentials and imposes significant limitations on the ability to analyze film growth processes on macroscopic space-time scale. Methods of classical nucleation theory are often used to study the formation of continuous films [22–24]. The approaches of phase field theory [24–27] are also used making it possible to operate on a larger space-time scale compared to the atomic modeling methods. The methods

of phase field theory were used for the consistent analysis of phase diagrams and dynamics of phase transformations in single-component [24,25], as well as in two-component films, taking into account the processes of deposition and evaporation of molecules from the substrate surface [26]. In a number of other works, phase-field models have been used to describe the dendritic growth of isolated islands of two-dimensional materials [27].

In this paper, a theoretical study of the dynamics of two-dimensional material growth during continuous deposition and evaporation is carried out, starting from the stage of nucleation and ending with the formation of a continuous film. The study is carried out using methods of phase field theory, which allows us to directly account for the anisotropy of the 2D materials energy boundaries, as well as thermal fluctuations. Taking into account the anisotropy of the boundaries energy we may consider the symmetry of the material lattice, which can also lead to the appearance of faceted islands or pores formed at various stages of the synthesis of continuous films.

2. Phase-field model of epitaxial growth of the 2D materials

Let us consider the process of formation and growth of a two-dimensional material characterized by an anisotropic boundary energy on an ideal substrate in conditions of continuous deposition. We will characterize the considered system by the concentration $c = c(\mathbf{r}, t)$ of the precipitated substance (e.g., boron or carbon) and the order parameter $\phi = \phi(\mathbf{r}, t)$, which allows us to distinguish between disordered ($\phi = 0$) and ordered ($\phi = 1$) phases.

Using the general approaches of phase field theory, the free energy of a two-dimensional material can be defined as a functional

$$F = n_0 \int\limits_S \left(f(c, \phi) + \frac{1}{2}\varepsilon^2(\mathbf{n})(\nabla\phi)^2 + \frac{1}{2}\kappa(\nabla c)^2 \right) ds. \tag{1}$$

Here $f(c, \phi)$ is the free energy density, which takes into account the interaction of deposited atoms with the substrate and with each other, $\varepsilon^2(\mathbf{n})$ and κ are the gradient energy coefficients. In this case, the function $\varepsilon(\mathbf{n})$ depends on the position of the normal $\mathbf{n} = \{n_x, n_y\}$ to the edge of the order parameter ϕ [28–31] and is determined by the electronic structure of the material and the orientation properties of the substrate on which epitaxial growth is realized. The position of the normal can be related to the order parameter using the formula $\mathbf{n} = \widehat{\mathbf{R}}_\alpha \nabla\phi$, where $\widehat{\mathbf{R}}_\alpha$ is the rotation operator for an arbitrary constant angle α, which determines the orientation of the growing two-dimensional material relative to the substrate. Integration in the functional (1) is carried out over the entire area of the substrate S, on which a two-dimensional material is formed.

In the considered model, the free energy density reflects the presence of stable states corresponding to disordered A ($c \approx 0$, $\phi \approx 0$) and ordered B ($c \approx 1$, $\phi \approx 1$) phases. These two states are separated by a barrier, the overcoming of which requires the presence of supersaturation, as well as thermal fluctuations, allowing to overcome this barrier. At sufficiently large degrees of supersaturation corresponding to the region of unstable states, the phase transition may turn out to be non-activation one, which corresponds to the spinodal mechanism of phase formation.

The free energy density $f(c, \phi)$, reflecting the presence of stable states corresponding to the forming phases, can be written as

$$f(c, \phi) = f_{\mathrm{A}}(c)h(\phi) + f_{\mathrm{B}}(c)\big[1 - h(\phi)\big] + \frac{1}{4}W\phi^2(1-\phi)^2, \tag{2}$$

where $f_{\mathrm{A}}(c)$ and $f_{\mathrm{B}}(c)$ are the densities of free energy for the disordered and ordered states, respectively, W is the interaction parameter, $h(\phi) = \phi^2(3 - 2\phi)$ is the approximation function.

The free energy densities, taking into account the energies of atoms in various states, as well as the configuration entropy, can be written as expressions

$$f_i(c) = f_i^0 + f_i^1 c + f_i^2(1-c) + k_{\mathrm{B}}T\big[c\ln c + (1-c)\ln(1-c)\big], \quad i = \{\mathrm{A}, \mathrm{B}\}. \tag{3}$$

Here f_i^0, f_i^1 and f_i^2 are interaction parameters that determine the energy of atoms in the reviewed states, as well as taking into account their interaction with the substrate.

Examples of free energy density relief demonstrating the possibility of a phase transition between states A and B are shown in Figure 1. Since the paired interactions between particles is taken into account, it may result in the appearance of quadratic terms by concentration (see, for example, [26]) in the formula (3), which can lead to the emergence of additional stable states, e.g., ($c \approx 1$, $\phi \approx 0$). In this case, the phase transition can be carried out through an intermediate state, and the nucleation process can take place through a two-stage mechanism [32–36]. The modelling parameters are given in Table 1.

The anisotropy of the boundary energy for two-dimensional materials, taking into account different types of symmetry, can be expressed using general expression introduced in 2D model of non-isothermal crystallization developed by Kobayashi [28]:

$$\varepsilon = \varepsilon_0\big[1 + \delta\cos(K\theta)\big], \tag{4}$$

where ε_0 is a constant value that determines contribution of the gradient energy of the order parameter, δ is a constant dimensionless multiplier that determines the intensity of anisotropy, K is a multiplier corresponding to the order of the axis of symmetry. The angle of rotation of θ boundary depends on the position of the normal to the

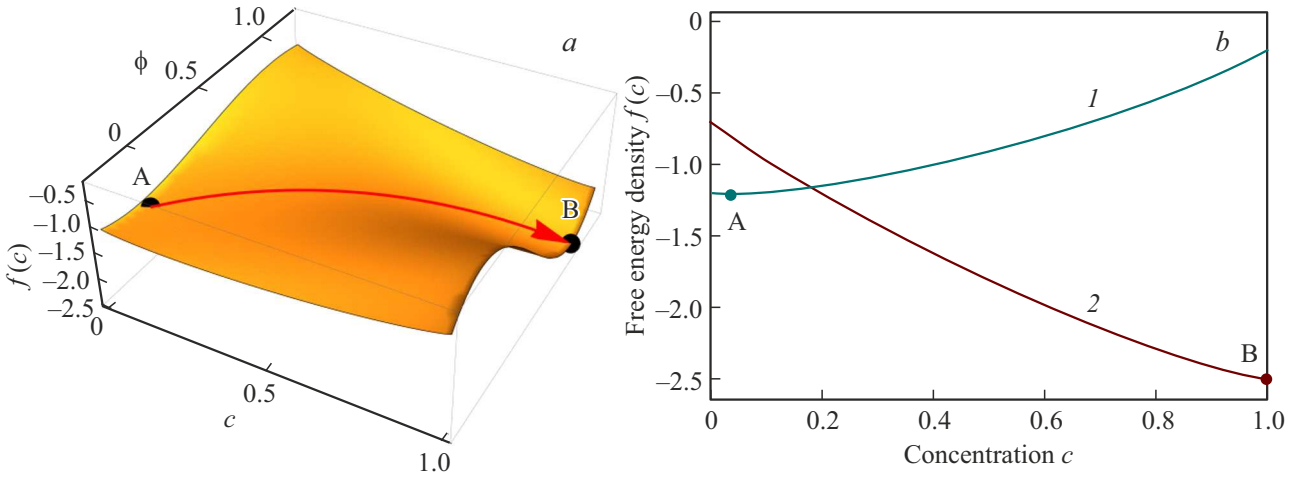

Figure 1. *a*) Density relief of free energy $f(c, \phi)$, reflecting the one-stage phase transition between the two steady states ($c \approx 0$, $\phi \approx 0$) and ($c \approx 1$, $\phi \approx 1$). *b*) Densities of free energy for the disordered ($f(c, 0)$ — curve *1*) and ordered ($f(c, 1)$ — curve *2*) of states. Points A and B denote the extremums of the free energy density.

Table 1. Phenomenological (dimensionless) parameters used for modelling

W	T	f_A^0	f_A^1	f_A^2	f_B^0	f_B^1	f_B^2	λ
1.0	0.3	−0.7	−1.8	0.0	0.0	−0.2	−1.2	0.1
κ	M_c	M_ϕ	I_+	I_-	K	τ_0	α	δ
0.0002	1.0	33.0	$2.0 \cdot 10^{-2}$	$0.0–7.0 \cdot 10^{-2}$	3	0.1	$\pi/4$	0.25
					6	0.2	$\pi/8$	0.45

Table 2. Analytical expressions for the function $a(\mathbf{n})$ at different values of K

K	Since function $a(n_x, n_y)$
3	$1 + \delta n_x(n_x^2 - 3n_y^2)/(n_x^2 + n_y^2)^{3/2}$
4	$1 - 3\delta + 4\delta(n_x^4 + n_y^4)/(n_x^2 + n_y^2)^2$
6	$1 + \delta(n_x^2 - n_y^2)(n_x^4 - 14n_x^2n_y^2 + n_y^4)/(n_x^2 + n_y^2)^3$

front, for which the expression $\cos(\theta) = n_x/\sqrt{n_x^2 + n_y^2}$ is valid. The energy anisotropy of the boundary of two-dimensional materials is characterized by the presence of symmetry axes of the third or sixth orders, therefore K can take values of 3 or 6. Cubic symmetry ($K = 4$) can also be observed for metals forming sub-monolayer films, which is most often discussed in the literature when solving problems of dendritic crystal growth [37–41]. Using the given values K, from the formula (3) and with the help of trigonometric transformations, it is possible to obtain analytical expressions for the anisotropy function of the boundary energy $a(\mathbf{n}) = \varepsilon(\mathbf{n})/\varepsilon_0$, shown in Table 2.

Further, we will consider the dynamics of film formation characterized by the anisotropy of the boundary energy $a(\mathbf{n})$ with the axis of symmetry of the third and sixth orders, which are most often observed for two-dimensional materials ($K = 3$ — h-BN, WS_2 [42], $K = 6$ — graphene, stripeline borophene [43]). Examples of functions $a(\mathbf{n})$ at given values K in polar coordinates are shown in Figure 2. For the spatial orientation of dependence $a(\mathbf{n})$ a rotation operator $\hat{\mathbf{R}}_\alpha$ to angle α in 2D space was applied.

Taking into account the conservativeness property of the concentration field and the non-conservativeness of the order parameter field, we can write the dynamic equations for these variables in the form

$$\left.\begin{aligned} \frac{\partial c}{\partial t} &= \nabla \cdot \left[M_c \nabla \frac{\delta F}{\delta c}\right] + I_+(1-c) + I_-\left[1 - h(\phi)\right]c + \nabla \cdot \boldsymbol{\xi} \\ a^2(\mathbf{n})\frac{\partial \phi}{\partial t} &= -M_\phi \frac{\delta F}{\delta \phi} + \xi \end{aligned}\right\}, \tag{5}$$

where M_c is the mobility of deposited atoms, M_ϕ is the order parameter relaxation constant, I_+ and I_- are the constants defining the rate of atoms deposition and evaporation from the substrate surface in the considered isothermal conditions, $\boldsymbol{\xi}$ and ξ are the random Gaussian fields providing the thermal fluctuations. The coefficients of deposition I_+ and evaporation I_- rates are determined by the flow and chemical potentials of the deposited atoms in the external environment and on the substrate, as well as by temperature [26]. At the same time, it is believed that the evaporation process mainly refers to atoms that have not passed into the phase of a two-dimensional material. When

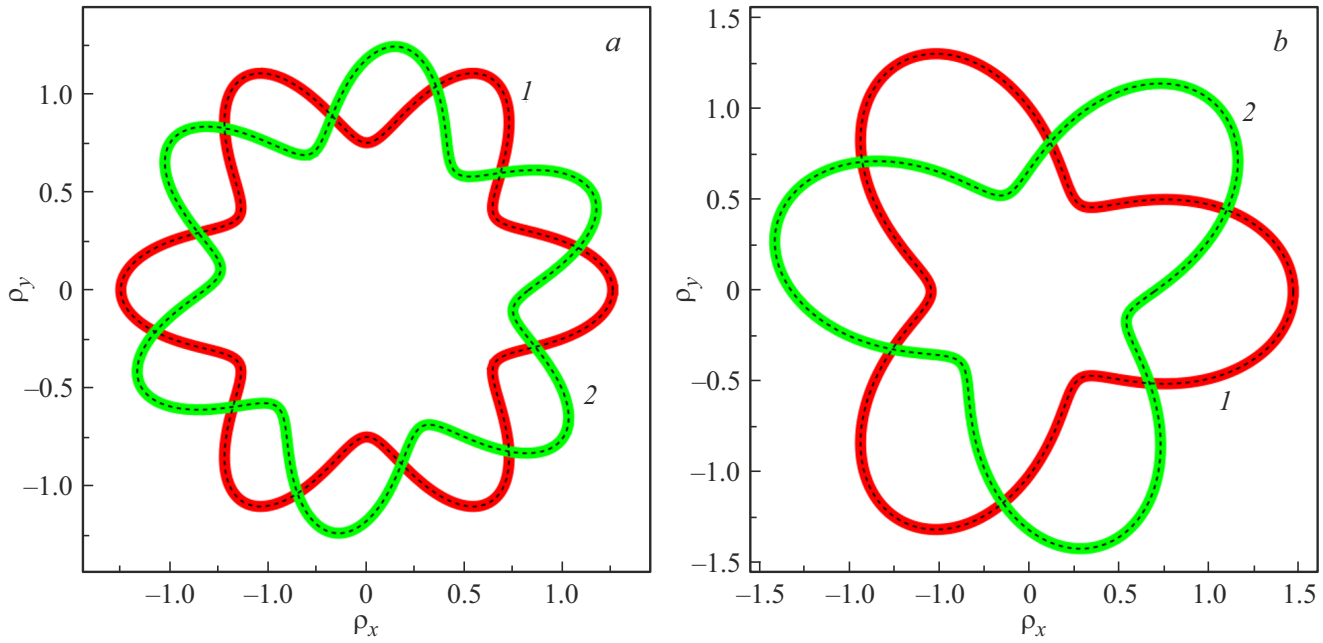

Figure 2. Function of surface energy anisotropy plotted as $\rho(n_x, n_y) = a(\mathbf{n})\{n_x, n_y\}$ at $n_x = \cos\psi$, $n_y = \sin\psi$ $(0 \le \psi \le 2\pi)$: *a*) $K = 6$, $\delta = 0.25$; *b*) $K = 3$, $\delta = 0.45$. Solid lines are calculated using formulae from Table 2: curve *1* — $\alpha = 0$, *2* — *a*) $\alpha = \pi/8$, *b*) $\alpha = \pi/4$. The dashed lines are obtained using the formula for the specified parameter value.

atoms are attached to the new phase growing islands, the appearance of new covalent bonds between the adsorbed atoms leads to a sharp decrease in the evaporation rate, the value of which can be neglected compared to evaporation of individual atoms that interact only with the substrate, forming, as a rule, relatively weak Van der Waals bonds. Since the evaporation of atoms from the formed two-dimensional phase is small, it can be expected that the degree of coating of substrate θ_c will asymptotically tend to unity during deposition (see also [26]). It should also be noted that multilayer two-dimensional materials (for example, multilayer graphene) can also be synthesized on substrates, however, interlayer bonds are also of Van der Waals type. These relatively weak interlayer bonds may be the reason for the high rate of atomic evaporation, which makes it possible to synthesize extended single-layer structures, which are considered in this study.

After calculating the variation derivatives in equations (5), we get equations of the form

$$\left.\begin{aligned} \frac{\partial c}{\partial t} &= \nabla\cdot\left[M_c\nabla\left\{\frac{\partial f}{\partial c} - \kappa\nabla^2 c\right\}\right] \\ &\quad + I_+(1-c) + I_-\left[1-h(\phi)\right]c + \nabla\cdot\boldsymbol{\xi} \\ a^2(\mathbf{n})\frac{\partial\phi}{\partial t} &= -M_\phi\left[\nabla\cdot\varepsilon^2\nabla\phi + \frac{\partial}{\partial x}\left\{(\nabla\phi)^2\varepsilon\frac{\partial\varepsilon}{\partial\phi_x}\right\}\right. \\ &\quad \left. + \frac{\partial}{\partial y}\left\{(\nabla\phi)^2\varepsilon\frac{\partial\varepsilon}{\partial\phi_y}\right\} - \frac{\partial f}{\partial\phi}\right] + \xi \end{aligned}\right\}. \quad (6)$$

The fluctuation terms in (6) are set using correlation functions [26,44]:

$$\left.\begin{aligned} \langle\xi_i(\mathbf{r},t),\xi_i(\mathbf{r}',t')\rangle &= 2M_c k_B T w(\mathbf{r}-\mathbf{r}')\delta(t-t')\delta_{ij} \\ \langle\xi(\mathbf{r},t),\xi(\mathbf{r}',t')\rangle &= 2M_\phi k_B T w(\mathbf{r}-\mathbf{r}')\delta(t-t') \end{aligned}\right\}. \quad (7)$$

where $\delta(t)$ is the delta-function, δ_{ij} is the Kronecker symbol, and the spatial correlation is set using Gaussian function [44]:

$$w(\mathbf{r}-\mathbf{r}') = \frac{1}{2\pi\lambda^2}\exp\left[-\frac{(\mathbf{r}-\mathbf{r}')^2}{2\lambda^2}\right], \quad (8)$$

λ is the correlation length. In the limit $\lambda \to 0$, the Gaussian function tends to the delta function, and the ratio (8) takes the form of a correlation function corresponding to white noise [45].

3. Numerical methods, model parameters, and boundary conditions

Further mathematical modeling of the two-dimensional materials growth during deposition is carried out in the following units:

$$\left.\begin{aligned} &[\mathbf{r}] = l, \quad [f] = W, \quad [T] = \frac{W}{k_B}, \quad [t] = n_0 W M_c/l^2 \\ &[M] = M_c, \quad [L] = M_c l^2, \quad [\kappa] = W l^2, \quad [I^\pm] = [t]^{-1} \end{aligned}\right\}, \quad (9)$$

where l is the spatial scale that was taken equal 10 nm.

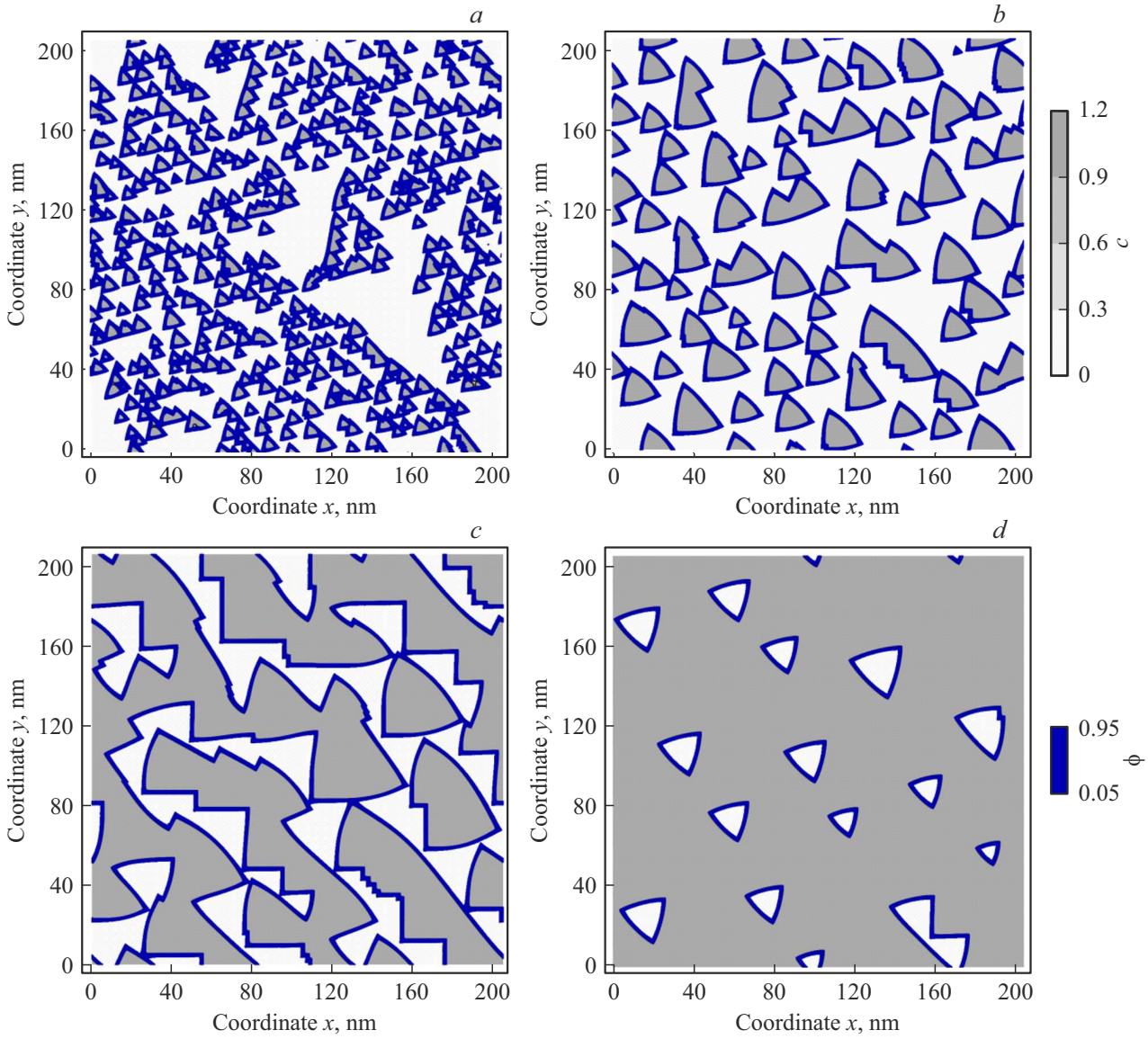

Figure 3. The history record of deposition of a solid layer of two-dimensional material having a third-order symmetry axis ($K = 3$) in the absence of evaporation ($I_- = 2 \cdot 10^{-3}$) at various time points t: *a*) 1.1 s, *b*) 1.8 s, *c*) 4.5 s, *d*) 10.1 s.

Solving a system of differential equations (6) was carried out using an explicit finite-difference Euler scheme on a rectangular homogeneous grid $S = 1024h \times 1024h$, where $h = 0.02l$ is the step of the spatial grid. The discretization of derivatives with respect to spatial variables was carried out using difference schemes [46–48], which ensure the isotropy of the corresponding differential operators. Periodic boundary conditions were applied. For each set of parameters $(50-125) \cdot 10^6$ iterations with a time spacing of $\Delta t = 2.0 \cdot 10^{-5}$ were implemented. The correlation length in dimensionless units was $\lambda \approx 0.1$. Modelling was carried out using Nvidia A100 graphics processing unit, and the calculations took about 40 h for the longest series of calculations.

Taking the diffusion coefficient of atoms over the substrate surface to be $D \approx 10^{-13}\,\mathrm{m^2/s}$, we can enter the time scale $\tau \approx n_0 M_c W/l^2 \approx c_0 DW/(k_B T l^2) \approx 0.009$ s, used to switch to dimensional units of time, c_0 is the equilibrium concentration of atoms on a substrate in the depleted phase.

4. Results of modelling and their discussion

Figures 3 and 4 show the results of simulating the formation and growth of two-dimensional materials on a substrate during continuous deposition at a low rate of atoms evaporation and various types of the order parameter anisotropy. At the initial stage of the deposition process, there are no islands of the new phase, and the system is characterized by an inhomogeneous distribution

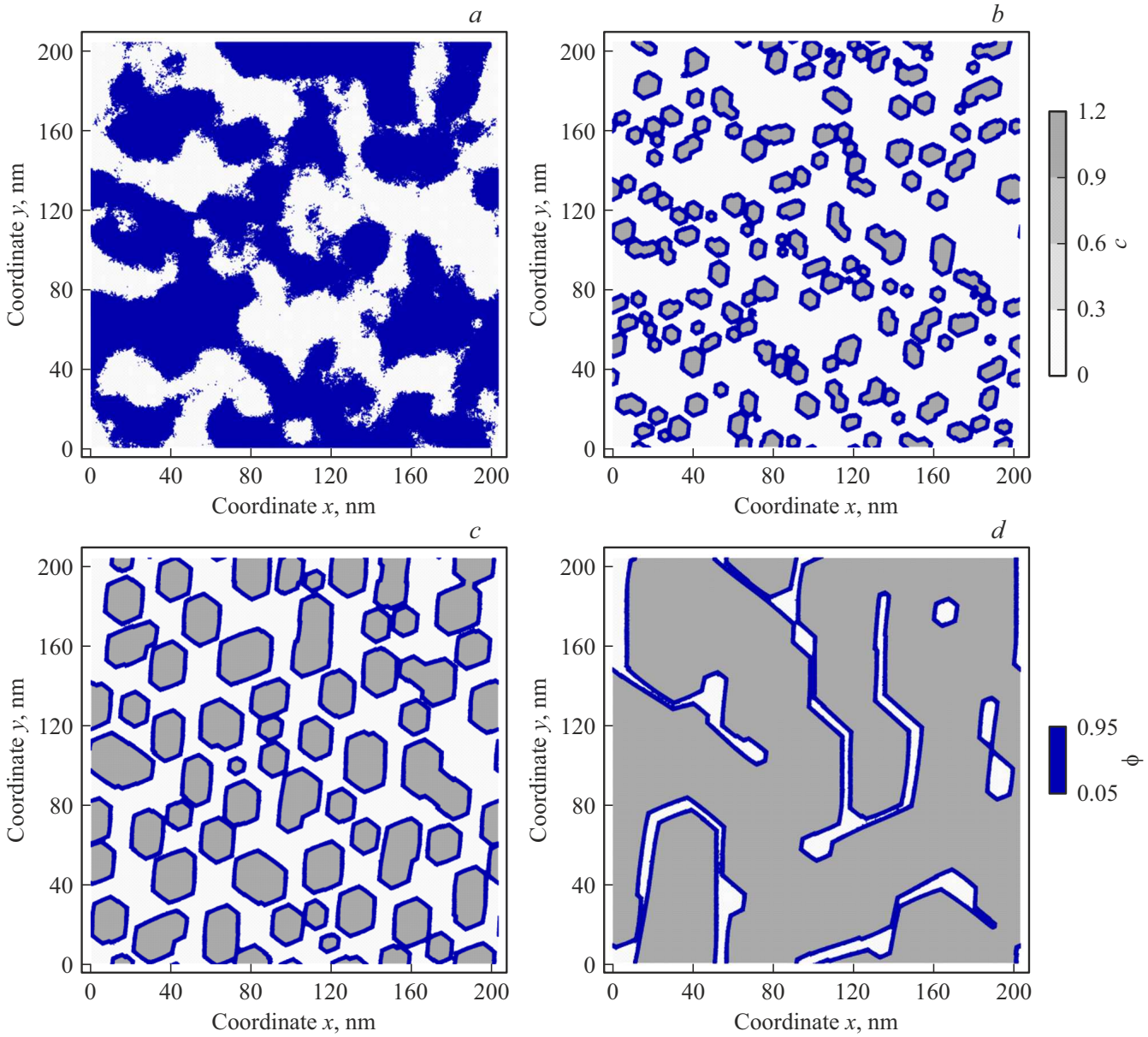

Figure 4. Dynamics of deposition of a continuous layer of two-dimensional material having a sixth-order symmetry axis ($K = 6$) in the presence of evaporation ($I_- = 8 \cdot 10^{-3}$) at various time points t: *a*) 1.1 s, *b*) 1.18 s, *c*) 2.7 s, *d*) 9.1 s.

of the concentration field and the order parameter due to fluctuations (see Figure 4, *a*). As the amount of precipitated substance grows, islands are formed either by the nucleation mechanism or by the non-activation (spinodal) mechanism. The implementation of one or another mechanism for the formation of a new two-dimensional phase depends on the deposition and evaporation rates. With a slow deposition process, overcoming the nucleation barrier, achieved during incubation time, can occur before reaching the metastability limit. With rapid deposition, the transition to the unstable state region may occur faster than the nucleation barrier is overcome, which can lead to the non-activation formation of a new phase.

When the new phase is being formed the generated islands have a triangular (Figure 3, *a*) and hexagon geometry (Figure 4, *b*) obtained due to anisotropy of the boundary energy. Due to this geometry, the developed model differs from the classical approaches of nucleation theory, where nuclei with circular (2D) or spherical (3D) symmetry peculiar to the isotropic boundary energy are mainly considered (i. e., at $\delta = 0$). In the process of atomic deposition and island growth, the coverage area becomes larger. Due to high concentration of nuclei formed, there is a high intensity of island fusion, which leads to an increase in their size and a decrease in surface concentration. Another mechanism, due to the diffusive transfer of matter between the islands (Ostwald ripening), was rather weakly manifested. This

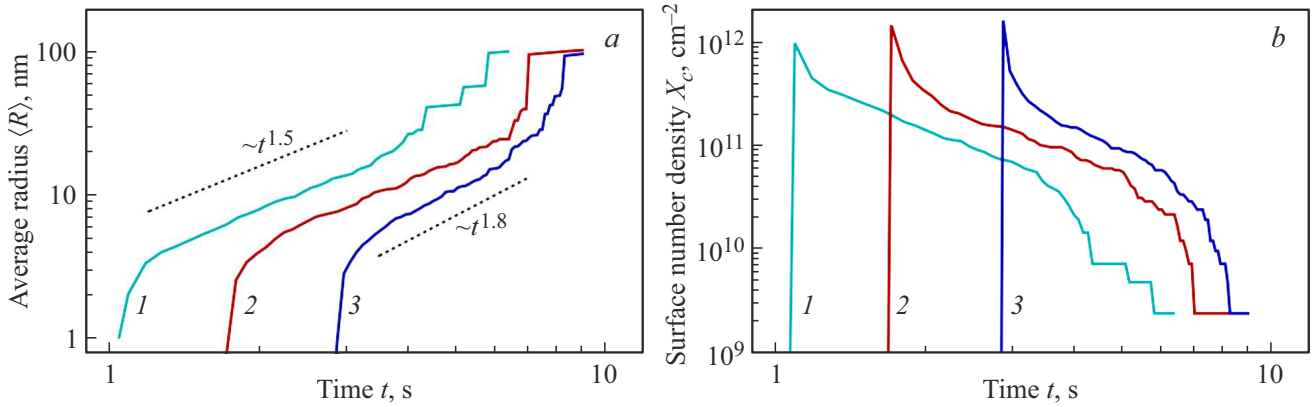

Figure 5. History records of *a*) average radius and *b*) surface concentration of the 2D material islands ($K = 3$) at different coefficients of the material evaporation rate I_-: curve *1* — $2.0 \cdot 10^{-3}$, *2* — $5.0 \cdot 10^{-2}$, *3* — $7.0 \cdot 10^{-2}$.

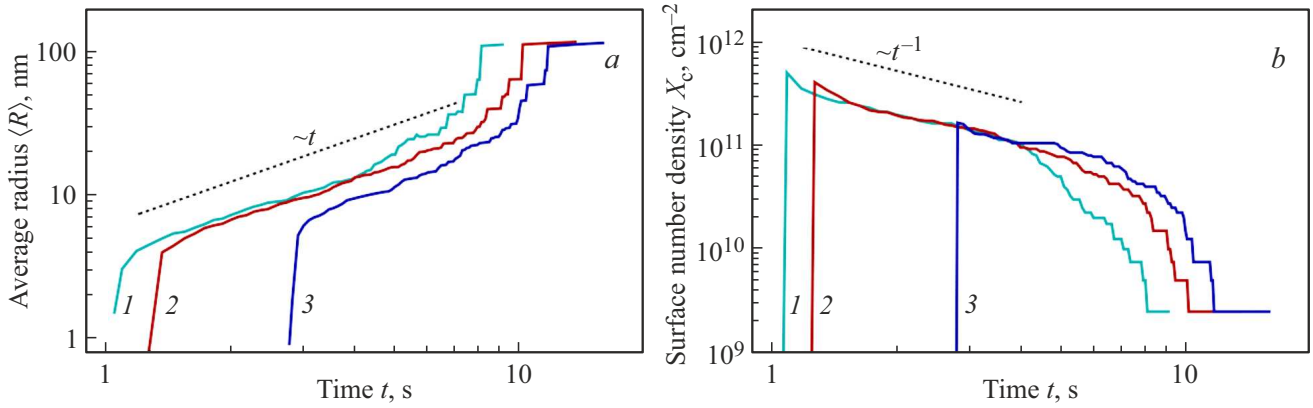

Figure 6. History records of *a*) average radius and *b*) surface concentration of the 2D material islands ($K = 6$) at different coefficients of the material evaporation rate I_-: curve *1* — 0.0 (without evaporation), *2* — $2.5 \cdot 10^{-2}$, *3* — $7.0 \cdot 10^{-2}$.

mechanism, studied in detail in [23–25], may be more pivotal in conditions of slower deposition.

In the process of merging the formed islands, a percolation structure is formed with a characteristic geometry corresponding to the selected type of anisotropy of the boundary energy (Figures 3, *c* and 4, *d*). A further increase in the degree of coating of the substrate leads to the formation of isolated pores having a geometry also determined by the function $\varepsilon(\mathbf{n})$ (Figures 3, *d* and 4, *d*).

Figures 5 and 6 show the dynamics of the average size and surface concentration of islands for the considered cases of boundary energy anisotropy ($K = 3$ and 6). Since the islands merging with each other is the dominant mechanism for the considered deposition and evaporation rates, the observed dynamics differs significantly from the well-known dependences described in the framework of diffusion growth or coalescence mechanisms [23]. For the considered growth of a two-dimensional material at $K = 3$, a very rapid growth of the average size $\langle R \rangle \propto t^{1.5-1.8}$ was observed with a sharply decreasing (hyperbolic) dependence of the surface concentration X_c. For $K = 6$ the observed growth rate appeared to be much lower: $\langle R \rangle \propto t$.

A similar phenomenon was discussed earlier in Smolukhovsky theory of rapid coagulation, in which the dynamics of island concentration can be described using the kinetic equation $dX_c/dt = -kX_c^2$ (k — kinetic coefficient). This equation leads to a simple qualitative dependence of the surface concentration on time $X_c(t) = X_c(t_0)\left[1 + kX_c(t_0)(t - t_0)\right]^{-1}$ (t_0 — initial moment of time) which is consistent with the data obtained based on the phase field theory (Figures 5 and 6).

Figure 7 shows the size distribution functions of the islands at various stages of the formation of a continuous layer of two-dimensional material. In conditions of intense island fusion at the considered stages, the maximum observed size does not exceed $(1.7-1.8)\langle R \rangle$.

One of the general-purpose approaches of the theory of phase transitions is Johnson–Mehl–Avrami-Kolmogorov model (JMAK), which allows analyzing the kinetics of the formed portion of a new phase using the ratio [49–51]

$$\theta_c = \theta_0\left[1 - \exp\left(-\{K_0 t\}^n\right)\right]. \qquad (10)$$

Here, θ_c is the portion of the new phase (coverage degree), θ_0 is the asymptotic value of the new phase portion

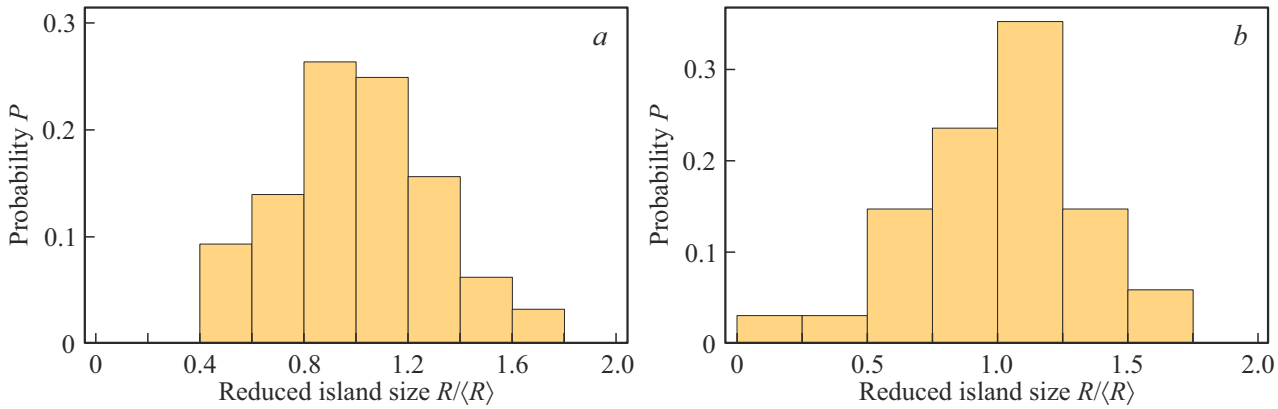

Figure 7. Size distribution functions of islands of two-dimensional material ($K = 6$) at evaporation rate of the material $I_- = 7.0 \cdot 10^{-2}$ at different time points: *a*) $t = 2.9$ s, *b*) $t = 5.5$ s.

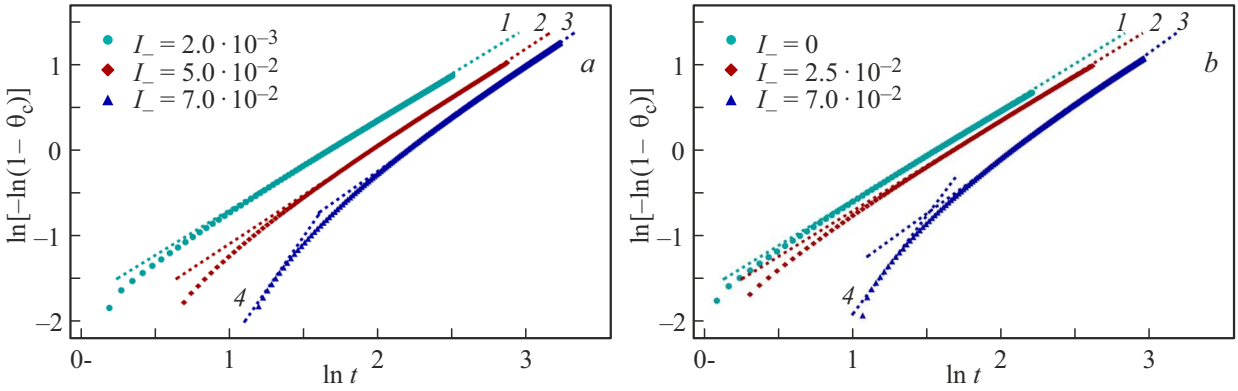

Figure 8. Substrate coverage area θ_c with a 2D material versus time t, s at various material evaporation rates (shown in the Figure). The dashed lines show the regions approximated by linear dependencies to determine n in formula (10). *a*) $K = 3$, curve *1* — $n = 1.06$, *2* — $n = 1.14$, *3* — $n = 1.22$, *4* — $n = 2.5$. *b*) $K = 6$, curve *1* — $n = 1.06$, *2* — $n = 1.06$, *3* — $n = 1.25$, *4* — $n = 2.3$.

($\theta_0 = 1$), K_0 is the constant, n is the Avrami exponent. The value of the indicator n depends on the dimension of the system and the mechanism of substance transfer between the islands. Also, the observed value of the exponent can be significantly influenced by the nature of the dependence of the rate of formation of a new phase on time [49–51]. Figure 8 shows the dependences θ_c obtained based on calculations performed for various evaporation rates I_-. As follows from the figure, at the stage of rapid fusion of the islands of the two-dimensional phase, this exponent has a value of $n \approx 1.06-1.25$. At an earlier stage (Figure 8, *a* and *b*, dashed lines *4*), when the processes of nucleation and diffusion growth are still underway, the value of the exponent can reach $n = 2.3-2.5$, which is consistent with the conclusions [49]. A comparative analysis of the phase-field modeling in the case of two-dimensional dendritic crystallization of alloys was carried out earlier in [51]. The history of Avrami exponent behavior at various stages of the phase transformation showed that the indicator has a non-monotonic dependence on time and in the later stages ($\theta \to \theta_0$) may decline to values $\sim 0.5-1.5$, which is also consistent with our results.

5. Conclusion

A phase-field model of the nucleation and growth of two-dimensional materials on the substrate surface during deposition has been developed. The model takes into account the anisotropy of the material boundary energy, which makes it possible to analyze the dynamics of formed islands characterized by axes of symmetry of the third or sixth orders observed in two-dimensional materials (graphene, borophene, transition metal dichalcogenides, etc.). Based on the results of modelling, the following conclusions can be made.

1. With rapid deposition and low evaporation rates, the main mechanism for the formation of continuous layers of two-dimensional material is the fusion of neighboring islands. Structural defects form in the area of fusion of neighboring islands, which are energetically unfavorable, which makes them a preferred place for joining new atoms. In the absence of mergers with other islands, these defects quickly overgrow, which leads to the relaxation of the island to a shape determined by the nature of the anisotropy of the boundary energy.

When implementing this mechanism of growth of a two-dimensional material, a high growth rate of the average size of islands $\langle R\rangle \propto t^{\alpha}$ $(\alpha = 1.0-1.8)$ was observed at the initial stage. At the late stage of the continuous film formation, there was a significant intensification of the fusion process and a significant acceleration in the growth of the average size.

2. At the stage when continuous layers of two-dimensional materials are formed, as a result of neighboring islands fusion, pores may form having a geometry characteristic of the boundary energy anisotropy inherent in the material. Some of the isolated pores may become of a regular shape during formation, characterized by the presence of axes of symmetry of the appropriate order.

3. Analysis of the portion of the formed two-dimensional phase showed that Avrami exponent depends on the coefficients of deposition and evaporation rates, and also goes down over time. At the early stage of film formation, where nucleation and growth processes dominate, the values of the $n \approx 2.3-2.5$ index were obtained. At a late stage, when the mechanism of merging of neighboring islands dominates, the values of the indicator decreased significantly, to values of $n \approx 1.06-1.25$.

Funding

The study was supported by the Russian Science Foundation (project No. 25-23-00077).

Conflict of interest

The authors declare that they have no conflict of interest.

References

[1] Carbon Nanomaterials Sourcebook, v. 1: Graphene, Fullerenes, Nanotubes, and Nanodiamonds / Ed. K.D. Sattler. CRC Press (2016). 630 p.
[2] H. Tetlow, J.P. De Boer, I.J. Ford, D.D. Vvedensky, J. Coraux, L. Kantorovich. Phys. Rep. **542**, *3*, 195 (2014).
[3] Y. Wang, X. Xu, J. Lu, M. Lin, Q. Bao, B. Özyilmaz, K.P. Loh. ACS Nano **4**, *10*, 6146 (2010).
[4] Z. Sofer, P. Šimek, V. Mazánek, F. Šembera, Z. Janoušek, M. Pumera. Chem. Commun. **51**, *26*, 5633 (2015).
[5] N.A. Vinogradov, A. Lyalin, T. Taketsugu, A.S. Vinogradov, A. Preobrajenski. ACS Nano **13**, *12*, 14511 (2019).
[6] Z. Xie, X. Meng, X. Li, W. Liang, W. Huang, K. Chen, J. Chen, C. Xing, M. Qiu, B. Zhang, G. Nie, N. Xie, X. Yan, H. Zhang. Res. **2020**, 2624617 (2020).
[7] M. Hakami, C.-C. Tseng, K. Nanjo, V. Tung, J.-H. Fu. MRS Bulletin **48**, *9*, 923 (2023).
[8] G. Xue, B. Qin, C. Ma, P. Yin, C. Liu, K. Liu. Chem. Rev. **124**, *17*, 9785 (2024).
[9] C. Herrmann, M. Raths, C. Kumpf, K.L. Kavanagh. Surf. Sci. **721**, 122080 (2022).
[10] M.M. Slepchenkov, P.V. Barkov, O.E. Glukhova. Micromachines **14**, *3*, 671 (2023).
[11] A.A. Kistanov, S.A. Shcherbinin, R. Botella, A. Davletshin, W. Cao. J. Phys. Chem. Lett. **13**, *9*, 2165 (2022).
[12] C. Fwalo, A. Kochaev, R.E. Mapasha. J. Energy Storage **84**, *Part B*, 110977 (2024).
[13] X. Liu, M.C. Hersam. Sci. Adv. **5**, *10*, aax6444 (2019).
[14] A. Kochaev, M. Maslov, K. Katin, V. Efimov, I. Efimova. Mater. Today Nano **20**, 100247 (2022).
[15] M.M. Slepchenkov, D.A. Kolosov, I.S. Nefedov, O.E. Glukhova. Mater. **15**, *24*, 8921 (2022).
[16] M.L. Pereira, E.J.A. dos Santos, L.A. Ribeiro, D.S. Galvão. Mater. Horiz. **12**, 1144 (2025).
[17] J.A. Baimova, S.A. Shcherbinin. Mater. **16**, *1*, 202 (2023).
[18] L.R. Safina, K.A. Krylova, J.A. Baimova. Mater. Today Phys. **28**, 100851 (2022).
[19] X. Ni, H. Huang, K.-H. Jin, Z. Wang, F. Liu. J. Phys. Chem. C **124**, *11*, 6063 (2020).
[20] R.A. Brazhe, A.I. Kochaev, A.A. Sovetkin. Phys. Solid State **55**, *9*, 1925 (2013).
[21] R.A. Brazhe, A.I. Kochaev, A.A. Sovetkin. Phys. Solid State **55**, *10*, 2094 (2013).
[22] S.A. Kukushkin, A.V. Osipov. Prog. Surf. Sci. **51**, *1*, 1 (1996).
[23] S.A. Kukushkin, V.V. Sleyozov, Dispersniye systemi na poverkhnosti tverdykh tel (evolutsionny podkhod). Nauka, SPb (1996).
[24] S.A. Kukushkin, A.V. Osipov. Phys. — Uspekhi **41**, *10*, 983 (1998).
[25] A.V. Osipov. J. Phys. D **28**, *8*, 1670 (1995).
[26] A.N. Saurov, P.E. L'vov, S.V. Bulyarskiy, V.V. Svetukhin. J. Mater. Chem. C **10**, *15*, 5864 (2022).
[27] E. Meca, J. Lowengrub, H. Kim, C. Mattevi, V.B. Shenoy. Nano Lett. **13**, *11*, 5692 (2013).
[28] R. Kobayashi. Phys. D **63**, *3–4*, 410 (1993).
[29] L. Gránásy, L. Rátkai, A. Szállás, B. Korbuly, G.I. Tóth, L. Környei, T. Pusztai. Metall. Mater. Trans. A **45**, *4*, 1694 (2013).
[30] L. Gránásy, G.I. Tóth, J.A. Warren, F. Podmaniczky, G. Tegze, L. Rátkai, T. Pusztai. Prog. Mater. Sci. **106**, 100569 (2019).
[31] W.J. Boettinger, J.A. Warren, C. Beckermann, A. Karma. Annu. Rev. Mater. Res. **32**, 163 (2002).
[32] D. Kashchiev. J. Cryst. Growth **530**, 125300 (2020).
[33] Y. Peng, F. Wang, Z. Wang, A.M. Alsayed, Z. Zhang, A.G. Yodh, Y. Han. Nature Mater. **14**, *1*, 101 (2014).
[34] P.E. L'vov, A.R. Umantsev. Crystal Growth & Design **21**, *1*, 366 (2021).
[35] W. Pan, A.B. Kolomeisky, P.G. Vekilov. J. Chem. Phys. **122**, *17*, 174905 (2005).
[36] S.A. Kukushkin, A.V. Osipov. Phys. Solid State **56**, *4*, 792 (2014).
[37] M. Asta, C. Beckermann, A. Karma, W. Kurz, R. Napolitano, M. Plapp, G. Purdy, M. Rappaz, R. Trivedi. Acta Materialia **57**, *4*, 941 (2009).
[38] Y. Zhao, K. Liu, H. Hou, L.-Q. Chen. Mater. & Design **216**, 110555 (2022).
[39] T. Takaki. ISIJ Int. **54**, *2*, 437 (2014).
[40] J. Kundin, I. Steinbach. Comp. Mater. Sci. **170**, 109197 (2019).
[41] M. Asta, J. Hoyt, A. Karma. Phys. Rev. B **66**, *10*, 100101(R) (2002).
[42] M. Hakami, C.-C. Tseng, K. Nanjo, V. Tung, J.-H. Fu. MRS Bulletin **48**, *9*, 923 (2023).

[43] L. Li, Q. Zhang, H. Li, D. Geng. Chem. Comm. **59**, *99*, 14636 (2023). https://doi.org/10.1039/d3cc04914k
[44] J. García-Ojalvo, J.M. Sancho. Noise in Spatially Extended Systems. Springer-Verlag, New York (1999).
[45] P.C. Hohenberg, B.I. Halperin. Rev. Mod. Phys. **49**, *3*, 435 (1977).
[46] B. Kamgar-Parsi, B. Kamgar-Parsi, A. Rosenfeld. IEEE Trans. Im. Proc. **8**, *10*, 1467 (1999).
[47] K. Ji, A. Malavi Tabrizi, A. Karma. J. Comp. Phys. **457**, 111069 (2021).
[48] A. Kumar. J. Comp. Phys. **201**, *1*, 109 (2004).
[49] J.W. Christian. The Theory of Transformations in Metals and Alloys. Pergamon, Amsterdam (2002).
[50] K. Shirzad, C. Viney. Royal Soc. Open Sci. **12**, *5*, 241696 (2025).
[51] J.J. Li, J.C. Wang, Q. Xu, G.C. Yang. Acta Materialia **55**, *3*, 825 (2007).

Translated by T.Zorina